ARTICLE

Kinking-Induced Structural Evolution of Metal Oxide Nanowires into Single-Crystalline Nanorings

Chaoyi Yan, Nandan Singh, and Pooi See Lee*

School of Materials Science and Engineering, Nanyang Technological University, Singapore 639798, Singapore

ABSTRACT We report an innovative method to fabricate single-crystalline nanorings based on the conventional vapor−liquid−solid (VLS) mechanism. The controllable formation of kinks in functional oxide nanowires (NWs) can be employed to fold the VLS-grown NWs into closed ring-shaped nanostructures. Successful syntheses of single-crystalline In_2O_3 and Zn_2GeO_4 nanorings were demonstrated. The present work provides an efficient method for nanoring fabrication based on NWs. The functional metal oxide nanomaterials with unique ring-shaped structures are expected to find interesting applications such as wave-guiding and photonic circuits.

KEYWORDS: metal oxide · nanoring · kink · nanowire · semiconductor · vapor−liquid−solid

Structure-controlled fabrication of semiconductor nanocrystals has attracted great interest because of their targeted applications in various fields, such as nanoelectronics,[1−3] optoelectronics,[4,5] and energy conversion.[6,7] Despite significant progress in past decades, fabrication of complex nanostructures in a controllable and predictable manner remains a challenge. In particular, the fabrication of semiconductor nanorings with high-crystallinity has been hindered owing to their unique geometrical shapes that would require unconventional synthetic approaches. Compared with template-assisted methods, the most frequently used approach for nanoring fabrication,[8−10] direct synthesis of closed ring-shaped nanostructures in vapor phase, is much more difficult. ZnO nanorings[11] were previously synthesized by epitaxial self-coiling of nanobelts driven by minimization of polar surface energy. However, the method is only applicable to certain material systems (such as those with polar facets). More importantly, the experimental conditions are challenging, and therefore this method[11] presents some difficulties to reproduce.

Developing a facile and efficient method for the synthesis of semiconductor nanorings would be of interest both for fundamental research and nanodevice applications. The vapor−liquid−solid (VLS) approach,[12] a versatile method that offers excellent control of the nanowire (NW) structural parameters,[13] has been widely employed for the synthesis of a broad range of functional oxide NWs.[14−17] In this report, we demonstrate kinking-induced structural evolution of VLS-grown metal oxide NWs into single-crystalline nanorings. We suggest that this method could potentially expand the generality of vapor-phase nanoring syntheses into a whole host of other shapes and forms. Conventionally, the VLS-grown NWs are usually straight throughout the length. It was recently shown, however, that it is possible to vary the NW growth direction by vapor perturbation, forming segmented NW chains.[18,19] Herein we show that the intentionally and controllably introduced kinks in NWs can be used to fabricate single-crystalline nanorings. The syntheses of two typical functional oxide nanorings (including binary In_2O_3 and ternary Zn_2GeO_4) are demonstrated. The facile and efficient method, described here, may not only facilitate the fabrication of a unique class of ring-shaped nanostructures, but also promote further studies of their properties and applications in functional nanodevices.

RESULTS AND DISCUSSION

First, the introduction of kinks in In_2O_3 NWs is demonstrated *via* pressure modulation. The resulting kinked In_2O_3 NWs can be categorized into two types: type I is the kinking of individual NW itself, and type II is branch kinking. Figure 1 panels a and b are the typical TEM image and corresponding electron diffraction (ED) pattern of the single-crystalline kinked individual NW. The

*Address correspondence to pslee@ntu.edu.sg.

Received for review April 27, 2010 and accepted August 27, 2010.

Published online September 9, 2010. 10.1021/nn101386c

NW is composed of multiple segments which show preferential perpendicular orientations to each other. The ED pattern (Figure 1b) along [101] zone axis indicates that the kinked segments in Figure 1a grow along the ⟨100⟩ and ⟨110⟩ directions of the cubic In_2O_3 phase (JCPDS 06-0416: a = 10.118 Å). More importantly, it reveals that the whole NW structure is single-crystalline despite the formation of multiple kinks. This was further confirmed by high-resolution TEM (HRTEM) analyses, where no bulk structural defects can be observed either in the straight segments or the joint sections (Figure S1, Supporting Information). Figure 1c is a typical example of type I kinking with ⟨100⟩/⟨100⟩ transitions. Growth directions of the kinked segments were identified from the corresponding ED pattern (Figure 1d) taken along [001] zone axis. The ED pattern also reveals clearly that the entire kinked NW structure is single-crystalline. Further examinations showed that all the type I kinking (also for type II kinking discussed below) exhibited exclusively either ⟨100⟩/⟨110⟩ or ⟨100⟩/⟨100⟩ transitions.

Interestingly, branched In_2O_3 NW heterostructures were also successfully synthesized by our one-step method with vapor perturbation, as shown in Figure 1e. Branch growth was guided by an Au catalyst, the dark particle on NW tip in Figure 1e inset. Unlike the growth under stable conditions, the vapor perturbation would lead to the split of the initial Au catalyst on the backbone tip. Consequently, the small Au clusters attached to the side-facets of the backbone may direct the homoepitaxial branch growth. It should be noted that no branched structures were obtained under stable growth conditions, such as, fixed pressure. This vapor perturbation induced Au split and branch formation may shed light on an innovative and facile method for the fabrication of branched metal oxide NW heterostructures. One-step synthesis of branched Si NWs were reported previously[20] due to the Au migration on NW surface.[20,21] However, the migration would be prohibited at certain conditions, such as oxygen-abundant environments,[20,22] and limit its applicability on metal oxide NWs. The present method could serve as an alternative method for one-step growth of branched In_2O_3 NWs, and may potentially be extended to other oxide materials. It should be noted that the pressure modulation induced kink formation was also observed in the branches (Figure 1e), analogous to the kinking of NW backbones shown in Figure 1a,c. The corresponding ED pattern of the branched NW is shown in Figure 1f. The regularly dotted pattern shows that the branches grew epitaxially on the backbone. The ED pattern also shows that the branches (with two segments) were kinking along the equivalent ⟨100⟩ directions. Analogous to type I kinking, ⟨100⟩/⟨110⟩ transition was also observed for type II branch kinking, as shown in Figure 3.

Comparative experiments were carried out to elucidate the effect of pressure on In_2O_3 NW growth. Different growth experiments were performed at constant pressure (0.02 and 1.9 mbar, respectively) for 60 min, with the other growth conditions kept constant. The results are shown in Figure S2, Supporting Information. While straight and dense In_2O_3 NW arrays were grown at 1.9 mbar, only thin films associated with microparticles were deposited at 0.02 mbar, indicating a slow deposition process at low pressure, probably dominated by the vapor−solid (VS) mechanism. The Au-catalyzed NWs obtained under constant growth conditions exhibited exclusively ⟨100⟩ growth directions (Figure S2, Supporting Information), and are straight without kinking. Kinked In_2O_3 NWs can only be obtained with vapor perturbation during growth (Figure 1).

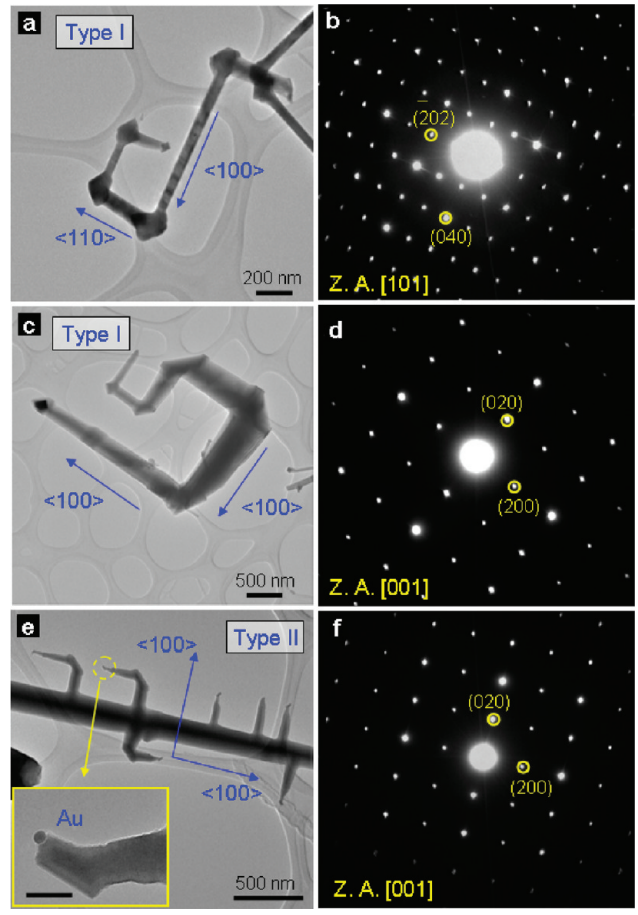

Figure 1. TEM images and corresponding ED patterns of single-crystalline kinked In_2O_3 nanowires. (a,b) Type I kinking with ⟨100⟩/⟨110⟩ transitions. (c,d) Type I kinking with ⟨100⟩/⟨100⟩ transitions. (e,f) Type II kinking with ⟨100⟩/⟨100⟩ transitions. Inset in panel e is an enlarged view of the Au catalyst at the branch tip. Scale bar is 20 nm. The ED patterns in panels b, d, and f were taken along [101], [001], and [001] zone axes, respectively.

The formation processes for the single-crystalline kinked In_2O_3 NWs can be described as follows: Initially the straight In_2O_3 NWs deposited at 1.9 mbar grew preferentially along ⟨100⟩ directions, as has been observed in previous reports.[23,24] At this point, the Ar gas was stopped during the perturbation phase, with the pressure reduced to ~0.03 mbar. While the partial pressure

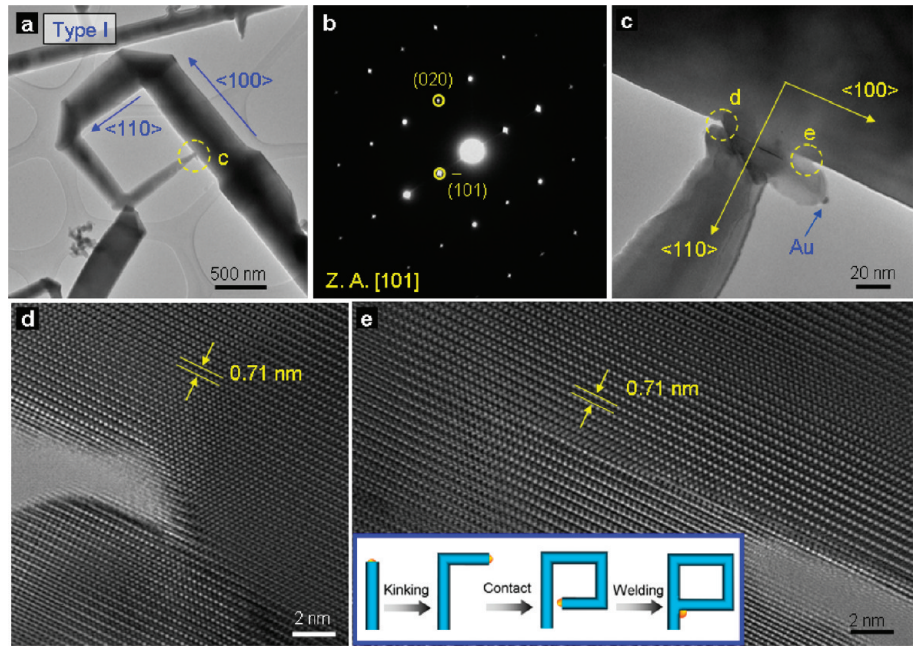

Figure 2. Detailed structures of the type I nanorings formed by NW self-welding: (a) TEM image and (b) ED pattern of a typical single-crystalline type I nanoring; (c) enlarged view of the tip-backbone joint section. Au catalyst can be viewed at the growth front. (d,e) HRTEM images of the joint sections, showing the defect-free crystallographic structure. Inset in panel e is the schematic diagram of the type I nanoring formation processes.

of In vapor was essentially unchanged under the constant evaporation temperature, the modulation of total pressure changed the mean free path of In vapor;[20] that is, the In vapor supply decreased with reduced total pressure, resulting in a lower supersaturation value in the catalyst particle. Consequently, VLS growth (axial elongation) of the NWs decreased significantly or even ceased. When Ar gas was reintroduced into the furnace, the supersaturation value in the catalyst particles would increase gradually (from the low level at 0.03 mbar to the high level at 1.9 mbar). During this process, preferential nucleation at the three phase (vapor/solid NW/liquid catalyst) boundaries[25] gradually changes the catalyst orientation.[19] The NW would grow along another preferential direction (in our case, ⟨100⟩ or ⟨110⟩) when the supersaturation value resumed to its initial level before perturbation. We suggest that the driving force for the growth direction change is the thermodynamic nucleation behavior at the phase boundaries/interfaces. It is worth mentioning that Madras *et al*. recently demonstrated the growth of kinked Si NWs under stable conditions (with constant growth temperature and vapor pressure).[26] The kinking formation was attributed to the kinetic driving force correlated to the growth rate (mainly determined by pressure) and other thermally activated processes (such as Si precipitation at the liquid−solid interface).[26] However, we suggest that the formation of kinked In_2O_3 NWs is not kinetically induced, since the NWs grown under stable conditions are exclusively straight without kinks (Figure S2, Supporting Information).

We suggest that the controllable formation of NW kinks can be employed to fold NWs into single-crystalline nanorings. To demonstrate its feasibility, the successful synthesis of In_2O_3 nanorings is presented (Figures 2 and 3). Because the nanorings were structurally evolved from the kinked NWs, they are also categorized into two types correspondingly: type I nanorings formed by kinking and welding of an individual backbone NW (self-welding) and type II nanorings formed by branch kinking and welding. Detailed structural characterizations and formation processes of type I nanorings are shown in Figure 2. As shown in Figure 2e inset, the initially straight In_2O_3 NW would kink toward another perpendicular direction due to the vapor perturbation. It is possible that the kinked tip would contact and weld with its backbone after several perturbation cycles. A representative nanoring with 3 kinks is shown in Figure 2a. Its corresponding ED pattern (Figure 2b) reveals that the entire nanoring structure is single-crystalline, with the kinked segments growing along ⟨100⟩ and ⟨110⟩ directions. The formation of the square-shaped nanoring can be attributed to the preferential perpendicular kinking behavior for cubic In_2O_3 (see also Figure 1). The inner length of the square varies from 786 to 840 nm due to the tapering of the NW, which resulted from the uncatalyzed VS growth on the NW sidewall.[27] Here we focus on the structural analyses of the tip-backbone joint section, since we have already shown that the kinking does not introduce any structural defects (Figure 1 and Figure S1, Supporting Information). An enlarged view of the tip-backbone joint section is shown in Figure 2c. The tip growth direc-

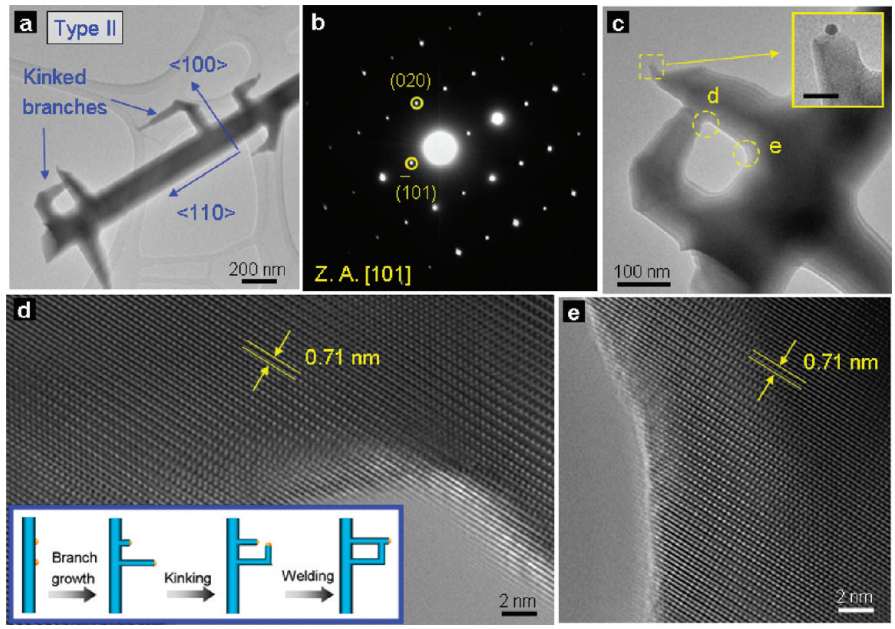

Figure 3. Detailed structures of the type II nanorings formed by branch-welding: (a) low-magnification TEM image; (b) ED pattern along [101] zone axis; (c) enlarged view of the nanoring. Inset shows the Au catalyst at the tip of the branch. Scale bar is 10 nm. (d,e) HRTEM images of the nanoring joints, showing the defect-free structure. Inset in panel d is the schematic diagram of the type II nanoring formation processes.

tion was redirected to ⟨100⟩ direction after being in contact with the backbone. The Au nanoparticle (diameter ~6 nm) verifies the VLS growth mechanism, as indicated by the arrow in Figure 2c. It should be noted that the tip successfully welded with the backbone and formed a closed single-crystalline nanoring structure. HRTEM images of the joint section are shown in Figure 2d,e. It can be clearly viewed that the tip and backbone exhibit the same atomic arrangements. More importantly, no structural defects, such as twin boundaries, were observed at the tip-backbone interface, which is a solid evidence for the formation of single-crystalline nanoring. The measured distance of 0.71 nm (Figure 2d,e) is consistent with the calculated spacing between adjacent (110) planes of cubic In_2O_3.

A schematic diagram of the formation processes of type II nanorings is shown in the Figure 3d inset. This type of nanorings was formed *via in situ* branch growth, kinking, and welding processes. The small Au clusters (originating from vapor perturbation induced Au splitting) would direct the homoepitaxial growth of branches. The branch may kink and weld with the other branches in the vicinity consequently, analogous to the individual NW in Figure 2. A representative low magnification TEM image of the type II nanoring is shown in Figure 3a, and an enlarged view is shown in Figure 3c. The Au catalyst particle can also be observed at the branch tip (Figure 3c inset). The entire nanoring structure is single-crystalline, as confirmed by the ED result (Figure 3b). The branches initially grew along ⟨100⟩ directions and then kinked toward ⟨110⟩ directions, parallel to the backbone NW. HRTEM images of the branch−branch and branch−backbone joint sections are shown in Figure 3 panels d and e, respectively. The clear and continuous lattice fringes verify the defect-free single-crystalline structure, consistent with ED result (Figure 3b).

One important phenomenon to be noted is the nanowelding process between the NW tip and backbone, which is critical for the formation of single-crystalline nanorings. A simplified model depicting the nanowelding process is shown in Figure 4. The Au tip would approach and contact with the backbone as the NW growth proceeds (step 1 and 2 in Figure 4). In step 3, it should be highlighted that precipitation occurs at both of the interfaces, that is, Au−tip and Au−backbone interfaces, due to the identical

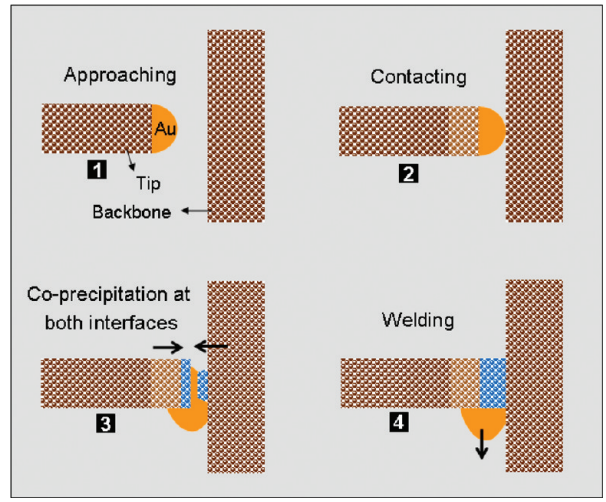

Figure 4. Schematic illustration of the nanowelding processes, including approaching (step 1), contacting (step 2), coprecipitation (step 3), and welding (step 4).

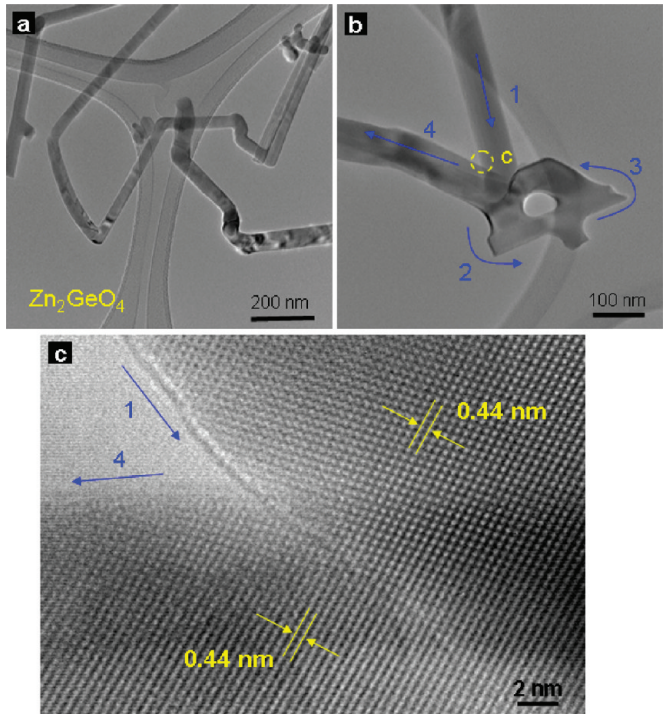

Figure 5. TEM and HRTEM images of single-crystalline kinked Zn_2GeO_4 NWs and nanorings. Unlike the preferential perpendicular kinking behavior for In_2O_3, irregular kinking was typically observed for Zn_2GeO_4 NWs, leading to the formation of circular nanorings.

Au−In_2O_3 interfacial conditions. The freshly grown segments from both sides would contact and coalescence into single-crystalline interfaces, as verified by HRTEM analyses shown in Figures 2 and 3. Previous studies showed that particle coalescence played an important role in the formation of single-crystalline nanocrystals,[28−30] and this was further verified by *in situ* TEM observations very recently.[31] Colloidal nanocrystals in contact with each other may merge into larger nanocrystals or more complex structures.[28−31] Similar phenomenon was also observed in vapor phase, where single-crystalline ZnO nanorings were formed by the contacting and coalescence of polar nanobelts.[11] We expect a similar merging process for the In_2O_3 NW tip and backbone when they are in contact at the high growth temperature region (320−410 °C). Moreover, the tip and backbone here are intersecting at the same crystallographic planes, since kinking does not introduce structural defects (Figure 1). Thus, the formation of single-crystalline interfaces can be readily expected according to the previous studies of oriented attachment.[28]

Another type of In_2O_3 nanorings formed by the welding of branch and backbone was also occasionally observed (Figure S3, Supporting Information). However, the frequency of occurrence is much lower than the type I and II nanorings shown above. Previously, regularly kinked zigzag chains were observed for the Si NWs grown by chemical vapor deposition (CVD).[19] We noticed, however, that there was no obvious tendency for the kinked In_2O_3 NWs to form regular zigzagged structures. For a typical growth round in this work, ~60% of the NWs were kinked, and part of the kinked NWs (~20%) formed closed ring-shaped structures. It is worth mentioning that not all the ring-shaped structures are fused/closed structures. In some cases, the NW segments may deviate from the 2D plane where the kinked NW lies in; and no welding happens at the tip-backbone crossover section. A typical example of the nonwelded nanoring is shown in Figure S4, Supporting Information. Although most of the kinked In_2O_3 NWs are 2D structures (Figure 1−3), 3D structures with part of the kinked segments growing out of the 2D plane were also observed (Figure S5, Supporting Information). Similar preferential kinking within a 2D plane was also observed previously for Si NWs although the underlying mechanisms are unclear at the current stage.[19]

We have also used our method to synthesize kinked NWs and nanorings of another more complex ternary oxide material—zinc germanate (Zn_2GeO_4). Figure 5a is a representative TEM image of the as-grown Zn_2GeO_4 NWs with multiple kinks. Note that in present work, the changes of growth directions are treated as kinks, and the kinked segments do not necessarily follow well-defined crystallographic directions. The entire kinked structure remains single-crystalline. We would like to highlight that the preferential kinking behavior is highly material-dependent. Unlike the strictly perpendicular kinking observed for In_2O_3 NWs (Figures 1−3), erratic kinking behaviors without obvious trends were typically observed for the ternary Zn_2GeO_4 NWs (Figure 5). Not only the kinking angles between straight segments showed large variations (Figure 5), erratically curved segments with "wormy" trajectories were also observed (Figure S6, Supporting Information). However, the exact reasons of why Zn_2GeO_4 NWs exhibited erratic kinking behaviors instead of growing along preferential directions are yet unclear and require further studies.

Successful welding of the kinked Zn_2GeO_4 NWs into single-crystalline nanorings is shown in Figure 5b. The numbers 1−4 indicate the sequential steps of the NW elongation and welding processes. Unlike the square-shaped In_2O_3 nanorings, the Zn_2GeO_4 nanoring shows a circular shape, due to the erratic kinking behavior. HRTEM image of the crossover point of the two overlapping segments (as indicated in Figure 5b) is shown in Figure 5c. The identical lattice fringes of the two segments reveal clearly the single-crystalline structure of the nanoring.

Finally, we compare our studies with literature. First, very limited studies were previously reported to synthesize free-standing nanorings in vapor phase. Wang *et al.* reported the synthesis of ZnO nanorings by epitaxial self-coiling of nanobelts.[11] However, the method is only applicable to certain material systems (such as those with polar surfaces). The present report demon-

strates an innovative route for nanoring synthesis, based on the kinking and welding of metal oxide NWs. It is expected to facilitate the nanoring syntheses considering the vast and well-established synthetic method for functional oxide NWs. Second, kinking was previously observed in Si NWs grown by CVD method, but no closed ring-shaped Si nanostructures were observed.[19,26] As has been discussed above, the nanowelding process is critical for the formation of closed single-crystalline structures. Successful welding of the tip and backbone (Figure 4) has a strict requirement of the interfacial conditions, such as chemical compositions and crystallographic orientations. Unlike metal oxide NWs, nanowelding of elemental NWs (such as Si, Ge) would be hindered since the NWs are usually associated with surface oxides.[32−34] Third, thermal evaporation, a simple, less-toxic and cost-effective method, has been widely used for metal oxide NW syntheses. It offers, however, less controllability over the NW structures than the CVD approach. For example, delicate modulations of the NW axial and longitude compositions and doping were achieved,[13,19] but this is not the case for NWs grown by thermal evaporation. Analogously, we have found that lengths of the In_2O_3 NW segments (Figure S7, Supporting Information) vary over a large range even for the same growth time, in spite of the fact that precise control of the segment lengths was achieved in CVD grown Si NWs.[19] The controllability could potentially be improved by growing oxide NWs using metalorganic CVD (MOCVD), which may also provide more flexibility for structural and compositional variations. Fourth, the present study of kinking-induced structural evolution would be of interest both for fundamental understanding and device applications. The kinked NWs provide ideal platforms for direct observation of oriented attachment in 1D nanomaterials, which has rarely been observed previously. Unlike the cases in nanoparticles,[28,29] oriented attachment of 1D NWs are less encountered probably due to the difficulty to contact two NWs with identical crystallographic facets. The single-crystalline nature of the kinked NW ensures that the two segments are intersecting strictly at identical crystallographic planes, enabling the successful formation of a defect-free interface (Figure 4). The kinked/curved NWs are also of interest for applications in future integrated photonic circuits.[35,36] The unique geometric structure of the kinked NWs can be used, for example, to guide light around sharp and even acute turns. Previously, NWs assembled into crossed structures were used for this purpose.[35] However, the processes required for NW assembly are usually time-consuming and probably low-yield. Instead, kinked oxide NWs are expected to serve as excellent alternative candidates. Moreover, the feasibility of synthesizing NWs with multiple kinks (Figure 1) enables easily the guiding of light around multiple turns, which is not readily achievable for assembled crossed-NWs.

CONCLUSIONS

We investigated the kinking-induced structural evolution of metal oxide NWs into single-crystalline nanorings. The controllable formation of kinks by vapor perturbation can be employed to fold VLS-grown metal oxide NWs into nanorings. Two types of typical kinking and welding behavior of In_2O_3 NWs were discussed. We explained in detail the nanowelding process, which is critical for the formation of closed single-crystalline structure. We also demonstrated the successful synthesis of complex ternary Zn_2GeO_4 kinked NWs and nanorings, although the preferential kinking behaviors were found to be strongly material-dependent. Fabrication of the unique kinked and ring-shaped semiconductor nanostructures based on the well-established and versatile VLS method is expected to facilitate further studies of structure-dependent properties, as well as their applications in functional electronic and optoelectronic nanodevices.

EXPERIMENTAL SECTION

The NW syntheses were based on a double-tube temperature-controlled quartz tube furnace as described previously.[17] Si substrates precoated with Au thin film (6 nm) were used to collect the products. In a typical synthesis process of single-crystalline In_2O_3 nanostructures, mixed In and carbon powder (weight ratio 2:1) was used as source material with Ar as carrier gas. Carbon would prevent the melted In from agglomeration and hence maintain constant vapor pressure. The furnace was heated up and held at 1000 °C. Then Ar gas was periodically switched on (200 sccm, pressure 1.9 mbar) and off (no Ar gas, background pressure 0.03 mbar) for typically 10 cycles. The gas was turned on for 5 min and off for 5 min in each cycle. The In_2O_3 nanostructures were grown at 320−410 °C. Zn_2GeO_4 nanostructures were deposited at 400−500 °C by evaporating mixed ZnO, GeO_2, and carbon powders (molar ratio 2:1:3) at 1000 °C. The perturbation conditions were kept the same as that for In_2O_3. The products were characterized by field-emission scanning electron microscopy (SEM, JEOL 7600F) and transmission electron microscopy (TEM, JEOL 2100F).

Acknowledgment. The authors thank X. W. Lu and M. F. Lin for their support and insightful discussions. C. Y. Yan and N. Singh thank NTU for research scholarship.

Supporting Information Available: Additional information described in the text. This material is available free of charge *via* the Internet at http://pubs.acs.org.

REFERENCES AND NOTES

1. Lu, W.; Lieber, C. M. Nanoelectronics From the Bottom Up. *Nat. Mater.* **2007**, *6*, 841–850.
2. Xiang, J.; Lu, W.; Hu, Y. J.; Wu, Y.; Yan, H.; Lieber, C. M. Ge/Si Nanowire Heterostructures as High-Performance Field-Effect Transistors. *Nature* **2006**, *441*, 489–493.
3. Comini, E.; Baratto, C.; Faglia, G.; Ferroni, M.; Vomiero, A.; Sberveglieri, G. Quasi-one-dimensional Metal Oxide Semiconductors: Preparation, Characterization, and Application as Chemical Sensors. *Prog. Mater. Sci.* **2009**, *54*, 1–67.

4. Duan, X. F.; Huang, Y.; Agarwal, R.; Lieber, C. M. Single-Nanowire Electrically Driven Lasers. *Nature* **2003**, *421*, 241–245.
5. Amos, F. F.; Morin, S. A.; Streifer, J. A.; Hamers, R. J.; Jin, S. Photodetector Arrays Directly Assembled onto Polymer Substrates From Aqueous Solution. *J. Am. Chem. Soc.* **2007**, *129*, 14296–14302.
6. Bierman, M. J.; Jin, S. Potential Applications of Hierarchical Branching Nanowires in Solar Energy Conversion. *Energy Environ. Sci.* **2009**, *2*, 1050–1059.
7. Law, M.; Greene, L. E.; Johnson, J. C.; Saykally, R.; Yang, P. D. Nanowire Dye-Sensitized Solar Cells. *Nat. Mater.* **2005**, *4*, 455–459.
8. Zhu, F. Q.; Fan, D. L.; Zhu, X. C.; Zhu, J. G.; Cammarata, R. C.; Chien, C. L. Ultrahigh-Density Arrays of Ferromagnetic Nanorings on Macroscopic Areas. *Adv. Mater.* **2004**, *16*, 2155–2159.
9. Chen, J. X.; Liao, W. S.; Chen, X.; Yang, T. L.; Wark, S. E.; Son, D. H.; Batteas, J. D.; Cremer, P. S. Evaporation-Induced Assembly of Quantum Dots into Nanorings. *ACS Nano* **2009**, *3*, 173–180.
10. Yu, X. D.; Zhang, H. G.; Oliverio, J. K.; Braun, P. V. Template-Assisted Three-Dimensional Nanolithography *via* Geometrically Irreversible Processing. *Nano Lett.* **2009**, *9*, 4424–4427.
11. Kong, X. Y.; Ding, Y.; Yang, R.; Wang, Z. L. Single-Crystal Nanorings Formed by Epitaxial Self-Coiling of Polar Nanobelts. *Science* **2004**, *303*, 1348–1351.
12. Wanger, R. S.; Ellis, W. C. Vapor−Liquid−Solid Mechanism of Single Crystal Growth. *Appl. Phys. Lett.* **1964**, *4*, 89–90.
13. Li, Y.; Qian, F.; Xiang, J.; Lieber, C. M. Nanowire Electronic and Optoelectronic Devices. *Mater. Today* **2006**, *9*, 18–27.
14. Yang, P. D.; Yan, H. Q.; Mao, S.; Russo, R.; Johnson, J.; Saykally, R.; Morris, N.; Pham, J.; He, R. R.; Choi, H. J. Controlled Growth of ZnO Nanowires and Their Optical Properties. *Adv. Funct. Mater.* **2002**, *12*, 323–331.
15. Li, C.; Zhang, D. H.; Han, S.; Liu, X. L.; Tang, T.; Zhou, C. W. Diameter-Controlled Growth of Single-Crystalline In_2O_3 Nanowires and Their Electronic Properties. *Adv. Mater.* **2003**, *15*, 143–146.
16. Liu, Z. Q.; Zhang, D. H.; Han, S.; Li, C.; Tang, T.; Jin, W.; Liu, X. L.; Lei, B.; Zhou, C. W. Laser Ablation Synthesis and Electron Transport Studies of Tin Oxide Nanowires. *Adv. Mater.* **2003**, *15*, 1754–1757.
17. Yan, C. Y.; Lee, P. S. Synthesis and Structure Characterization of Ternary Zn_2GeO_4 Nanowires by Chemical Vapor Transport. *J. Phys. Chem. C* **2009**, *113*, 14135–14139.
18. Lilach, Y.; Zhang, J. P.; Moskovits, M.; Kolmakov, A. Encoding Morphology in Oxide Nanostructures During Their Growth. *Nano Lett.* **2005**, *5*, 2019–2022.
19. Tian, B. Z.; Xie, P.; Kempa, T. J.; Bell, D. C.; Lieber, C. M. Single-Crystalline Kinked Semiconductor Nanowire Superstructures. *Nat. Nanotechnol.* **2009**, *4*, 824–829.
20. Kawashima, T.; Mizutani, T.; Nakagawa, T.; Torii, H.; Saitoh, T.; Komori, K.; Fujii, M. Control of Surface Migration of Gold Particles on Si Nanowires. *Nano Lett.* **2008**, *8*, 362–368.
21. Hannon, J. B.; Kodambaka, S.; Ross, F. M.; Tromp, R. M. The Influence of the Surface Migration of Gold on the Growth of Silicon Nanowires. *Nature* **2006**, *440*, 69–71.
22. Kodambaka, S.; Hannon, J. B.; Tromp, R. M.; Ross, F. M. Control of Si Nanowire Growth by Oxygen. *Nano Lett.* **2006**, *6*, 1292–1296.
23. Wan, Q.; Dattoli, E. N.; Fung, W. Y.; Guo, W.; Chen, Y. B.; Pan, X. Q.; Lu, W. High-Performance Transparent Conducting Oxide Nanowires. *Nano Lett.* **2006**, *6*, 2909–2915.
24. Wan, Q.; Wei, M.; Zhi, D.; MacManus-Driscoll, J. L.; Blamire, M. G. Epitaxial Growth of Vertically Aligned and Branched Single-Crystalline Tin-Doped Indium Oxide Nanowire Arrays. *Adv. Mater.* **2006**, *18*, 234–238.
25. Wacaser, B. A.; Dick, K. A.; Johansson, J.; Borgstrom, M. T.; Deppert, K.; Samuelson, L. Preferential Interface Nucleation: an Expansion of the VLS Growth Mechanism for Nanowires. *Adv. Mater.* **2009**, *21*, 153–165.
26. Madras, P.; Dailey, E.; Drucker, J. Kinetically Induced Kinking of Vapor−Liquid−Solid Grown Epitaxial Si Nanowires. *Nano Lett.* **2009**, *9*, 3826–3830.
27. Vomiero, A.; Ferroni, M.; Comini, E.; Faglia, G.; Sberveglieri, G. Insight into the Formation Mechanism of One-Dimensional Indium Oxide Wires. *Cryst. Growth Des.* **2010**, *10*, 140–145.
28. Penn, R. L.; Banfield, J. F. Imperfect Oriented Attachment: Dislocation Generation in Defect-Free Nanocrystals. *Science* **1998**, *281*, 969–971.
29. Cho, K. S.; Talapin, D. V.; Gaschler, W.; Murray, C. B. Designing PbSe Nanowires and Nanorings Through Oriented Attachment of Nanoparticles. *J. Am. Chem. Soc.* **2005**, *127*, 7140–7147.
30. Pacholski, C.; Kornowski, A.; Weller, H. Self-Assembly of ZnO: From Nanodots to Nanorods. *Angew. Chem., Int. Ed.* **2002**, *41*, 1188–1191.
31. Zheng, H. M.; Smith, R. K.; Jun, Y. W.; Kisielowski, C.; Dahmen, U.; Alivisatos, A. P. Observation of Single Colloidal Platinum Nanocrystal Growth Trajectories. *Science* **2009**, *324*, 1309–1312.
32. Yan, C. Y.; Lee, P. S. Bismuth-Catalyzed Growth of Germanium Nanowires in Vapor Phase. *J. Phys. Chem. C* **2009**, *113*, 2208–2211.
33. Yan, C. Y.; Chan, M. Y.; Zhang, T.; Lee, P. S. Catalytic Growth of Germanium Oxide Nanowires, Nanotubes, and Germanium Nanowires: Temperature-Dependent Effect. *J. Phys. Chem. C* **2009**, *113*, 1705–1708.
34. Morales, A. M.; Lieber, C. M. A Laser Ablation Method for the Synthesis of Crystalline Semiconductor Nanowires. *Science* **1998**, *279*, 208–211.
35. Barrelet, C. J.; Greytak, A. B.; Lieber, C. M. Nanowire Photonic Circuit Elements. *Nano Lett.* **2004**, *4*, 1981–1985.
36. Yang, P. D.; Yan, R. X.; Fardy, M. Semiconductor Nanowire: What's Next. *Nano Lett.* **2010**, *10*, 1529–1536.